Mammalian tissue specific translation regulation; role of tRNA epitranscriptome in regulating codon optimality patterns across tissues.

Daisuke Ando[1,2]*. Sherif Rashad[2,3]#*. Thomas J Begley[4]. Hidenori Endo[5]. Masashi Aoki[1]. Peter C Dedon[6]. Kuniyasu Niizuma[2,3,5].

1) Department of Neurology, Tohoku University Graduate School of Medicine, Sendai, Japan

2) Department of Neurosurgical Engineering and Translational Neuroscience, Tohoku University Graduate School of Medicine, Sendai, Japan

3) Department of Neurosurgical Engineering and Translational Neuroscience, Graduate School of Biomedical Engineering, Tohoku University, Sendai, Japan

4) Department of Biological Sciences, University at Albany, Albany, NY, USA

5) Department of Neurosurgery, Tohoku University Graduate School of Medicine, Sendai, Japan

6) Department of Biological Engineering, Massachusetts Institute of Technology, MA, USA

*** These authors contributed equally.**

#Corresponding author:

Sherif Rashad, MD, PhD.

Email: sherif.mohamed.rashad.e3@tohoku.ac.jp

Abstract

The tRNA epitranscriptome has been recognized as an important player in mRNA translation regulation. tRNA modifications, tRNA expression, and tRNA derived small RNAs (tsRNAs) all play important roles in physiology as well as in multiple pathologies. While the decoding capacity of tRNA is generally understood, there remains gaps in our knowledge of the role of various tRNA processes in fine-tuning translation at the codon level. Specifically, how tRNAs regulates codon usage and bias at the tissue or cell levels remain unexplored. Here, we analyzed seven tissues from mice for the expression of tRNA modifications, mature tRNAs, and tsRNAs. We combined our analysis with Ribo-seq and evaluated various metrics for codon usage and optimality between tissues. Our analysis revealed distinct enrichment patterns of tRNA modifications in tissues. For example, queuosine and mcm5U modifications were most enriched in the brain. In addition, we observed lower levels of tRNAs and tsRNAs in the spleen with higher levels of snRNAs and snoRNAs compared to other tissues. Using three different metrics for codon analysis; isoacceptors frequencies, total codon frequencies, and A-site pausing, we revealed a strong A/T vs G/C ending codons bias in most tissues. The brain was the least biased tissue and was unique compared to all other tissues on multiple levels. Finally, we observed a strong concordance between the expression of queuosine modifications and the optimality of their decoded codons. Our results reveal that tRNA modifications are master regulators of translation and codon usage and optimality across tissues.

Keywords: tRNA modifications; Queuosine; Codon optimality; Ribosome profiling; translation.

Introduction

The translation of the gene code to functional protein is at the heart of all processes of life. This multistep process that starts from transcription all the way to post-translational protein modifications is under heavy regulation at each step. At the heart of this process lies mRNA translation, which is one of the most complex and heavily regulated processes. mRNA modifications and structure(Mao et al., 2019; Mauger et al., 2019), ribosome assembly and modifications(Sharma et al., 2018), and tRNA epitranscriptome(Suzuki, 2021) are few of the factors that interplay to regulate proper mRNA translation and proteostasis. In recent years, there has been an increased interest in the complexity and regulatory roles of tRNA epitranscriptome on mRNA translation(Nedialkova and Leidel, 2015; Suzuki, 2021). Importantly, alteration of tRNA expression(Goodarzi et al., 2016; Torrent et al., 2018), tRNA derived small non-coding RNAs (tsRNAs)(Liu et al., 2022a), and tRNA modifications(Rosselló-Tortella et al., 2020) were shown to impact mRNA translation and play roles in diseases such as cancer, metabolic disorders, and neuropsychiatric disorders(Dedon and Begley, 2022; Goodarzi et al., 2016; Liu et al., 2022a; Matsumura et al., 2023; Rosselló-Tortella et al., 2020; Zuko et al., 2021). However, our understanding of how tRNA epitranscriptome regulates mRNA translation, while substantially improved over the past years, is far from complete.

An interesting aspect of tRNA is that only 48 tRNA anticodons, in humans, decode 64 codons in the mRNA(Chan and Lowe, 2016). To compensate for this mismatch, non-cognate codon recognition at the wobble position, in accordance with Crick's rules, allows the decoding of the codons via the limited available tRNA pool(Crick, 1966; Suzuki, 2021). This process is regulated heavily by tRNA modifications at the wobble position, position 34(Huber et al., 2022; Nedialkova and Leidel, 2015; Suzuki, 2021). For example, tRNA modifications can expand or restrict the codon decoding by anticodons(Suzuki, 2021). A

famous example is Adenosine-to-Inosine conversion (A-to-I) which expands the recognition of NNU codons by ANN anticodons to NNU, NNC, and NNA by INN anticodons(Murphy and Ramakrishnan, 2004; Suzuki, 2021).

While several efforts have elucidated the dynamic nature of tRNA epitranscriptome in regulating processes such as the stress response(Endres et al., 2015; Huber et al., 2022; Rashad et al., 2020a; Rashad et al., 2021; Torrent et al., 2018) and growth conditions(Deng et al., 2015) and how these dynamic changes impact codon recognition(Chan et al., 2012; Torrent et al., 2018), much remains to be elucidated on the role of tRNA epitranscriptome in regulating physiologic mRNA translation in various tissues and cells and how such regulation can impact the function of these tissues. Several groups analyzed tRNA modifications(Guo et al., 2023) and tRNA expression(Pinkard et al., 2020; Yu et al., 2022) in mice tissues in order to elucidate such regulation. While these efforts did reveal important phenomena on tissue specific expression of tRNA epitranscriptome and its potential links to mRNA translation, they were limited in focusing on only one aspect of tRNA epitranscriptome at a time or not providing direct correlation with mRNA translation and codon decoding. In addition, the codon metrics used for the analysis in some works still require revisiting.

Here, we analyzed tRNA epitranscriptome (modifications, mature tRNA expression, and tsRNAs) from 7 mouse tissues using various methods [Figure 1a]. We combined our analysis with Ribo-seq analysis and applied various codon metrics to our dataset to reveal that tRNA modifications are master regulators of codon usage and optimality in various tissues. Our work also reveals interesting differences in the expression of tRNA modifications, tsRNAs, and other non-coding small RNAs between tissues that can be traced back to specific functional or physiological aspects of said tissues.

Results

➢ Tissue specific tRNA modification patterns

We first began by exploring the tRNA modifications landscape in each of the 7 tissues used in this study [Figure 1a]. Using high throughput LC-MS/MS, we were able to detect 45 known mammalian modifications that occur in the tRNA or in other small non-coding RNAs (such as m6A and m66A(Oerum et al., 2021; Suzuki, 2021)) [Supplementary figure 1a, supplementary table 1](Suzuki, 2021). Our results revealed significant tissue specific enrichment of certain modifications as well as tissue and modification clustering patterns [Figure 1b, supplementary table 2]. In addition, a cluster of related modifications, mcm5U, mcm5Um, and ncm5Um, which are regulated by the same enzyme system(Suzuki, 2021; van den Born et al., 2011) were also most enriched in the brain as well as queuosine (tRNA-Q) and its derivative mannosyl queuosine (manQ) but not its galactosyl derivative (galQ). We also observed that f5C and f5Cm, which exist in mitochondrial tRNA-Met and cytosolic tRNA-Leu^{CAA} (Kawarada et al., 2017) were most enriched in the heart and muscle. On the other hand, the liver and spleen had lower levels of almost all modifications, albeit the spleen showed an enrichment in a specific set of modifications that include 2'O-ribose modified nucleotides such as Cm, Gm, and Am, as well as several modifications not known to occur in the tRNA such as m66A and m6Am(Oerum et al., 2021; Suzuki, 2021) but occur in other small non-coding RNAs that elute with the tRNA enriched fraction as per the method used herein.

Next, we directed our attention to how tissues cluster and correlate with each other, which can give an idea about the fine-tuning of tRNA modifications towards tissue specific functions. To that end, we conducted Pearson's correlation [Figure 1c] and partial least square regression discriminant analysis (PLS-DA) [Figure 1d] to

understand such relations between tissues. Peason's correlation revealed that the brain had higher correlation with the kidney while it had a negative correlation with the spleen and lungs and no correlation with the liver [Figure 1c]. PLS-DA analysis [Figure 1d] confirmed the relationship between tissues, revealing that the brain clusters closely with the kidney while the lung, spleen, muscles, and heart formed another cluster. Further analysis of the distribution of modifications in the PLS-DA plot [Supplementary figure 1b], revealed how clusters of modifications correlated with tissue clusters. In addition, VIP analysis [Supplementary figure 1c] revealed important contributors to each tissue cluster expression pattern. For example, m66A contributed to the Spleen and Lung clustering patterns while tRNA-Q contributed to the brain followed by kidneys as discussed above. In addition to tissue clustering, we analyzed the correlation between tRNA modifications [Figure 1e]. Our analysis revealed clusters of modifications that follow the same expression patterns. For example, methylation modifications, such as m1A, m5C, m3C, etc., generally clustered together, while 2'O-ribose modifications clustered together and so on.

- **Tissue specific tRNA and anticodon patterns.**

  In this step, we directed our attention to the expression of mature tRNAs and their respective anticodons as well as other small non-coding RNAs, in particular; tsRNAs. We utilized ARM-tRNA-seq(Cozen et al., 2015) with few modifications, which revealed tissue specific variations in the expression of various non-coding RNAs. For example, the spleen showed very low levels of tRNAs compared to other tissues, while it has significantly higher snRNAs and snoRNAs [Figure 2a]. This pattern was also evident when RNA samples were analyzed using Bioanalyzer [Supplementary figure 2]. The lung also showed higher levels of snRNAs. This pattern can explain the enrichment of non-tRNA modifications in the spleen and lung compared to other

tissues. In addition, mitochondrial tRNAs (Mt_tRNA) were expressed in the heart at much higher levels, consistent with the enrichment of mitochondria related tRNA modifications observed above. We also observed notable differences in the ratios of tRNAs pertaining to particular amino acids within each tissue. Notably, Selenocysteine (SeC) representation was higher in spleen and lung, which can be related to the known immune functions of SeC and selenium intake[27]. Next, we collapsed the mature tRNA counts by anticodon and calculated the z-scores for the expression of different tRNAs across tissues [Figure 2d] and within each tissue [Figure 2c]. As reported previously(Pinkard et al., 2020), the relative expression of different tRNA isodecoders within each tissue were relatively stable. However, when comparing the relative expression of each isodecoder across tissues [Figure 2d] differences start to appear. Indeed, given the low expression of tRNAs in the spleen, almost all isodecoders were expressed at lower levels compared to other tissues, except for Ser^{CGA}. Further, despite the representation of SeC amino acid related counts in the spleen and lungs [Figure 2b], the isodecoder for SeC (SeC^{TCA}) was most expressed in the kidney. This might be attributed to how the tRAX software used in this analysis attributes the amino acid counts where tsRNAs are also incorporated in such counting process(Li et al., 2022). We also analyzed the expression of tRNA-Q modified tRNAs. Asp^{GTC} was most enriched in the kidneys, while Asn^{GTT} was equally enriched in both the Kidney and brain. On the other hand, His^{GTG} was equally expressed across tissues except in lung and spleen where it was expressed at lower levels. Paradoxically, Tyr^{GTA} was most expressed in the liver and underrepresented in the brain. This can be explained, however, by the lower expressed of galactosyl-queuosine modification in the brain which occurs in Tyr^{GTA} (Suzuki, 2021). Pearson's correlation analysis [Figure 2e] revealed a different pattern of clustering compared to

what was observed at the level of tRNA modifications. For example, the brain had modest positive correlation with the heart and liver, while it correlated negatively with the kidneys. These changes, however, remain subtle, as when analyzing the correlation between tissues using normalized read counts, there is near perfect correlation [Figure 2f].

While the isoacceptors cytosolic tRNAs expression were nearly uniform across tissues, mitochondrial tRNAs revealed a difference picture, where the heart showed much higher normalized read counts compared to all other tissues for almost all detected Mt-tRNAs with only a few exceptions [Supplementary figures 3a and 3b] and tissue specific clustering was observed [Supplementary figure 3c].

- **Tissue specific expression of tsRNAs**

We next directed our attention to another layer in the tRNA epitranscriptome. We evaluated the expression of various tsRNAs subtypes, namely tRNA halves (tiRNAs) and tRNA derived fragments (tRFs) which are processed via different enzymes and have different modes of action(Rashad et al., 2020b) [Figure 3a]. Analysis of the expression of various tsRNAs (tiRNAs and tRFs) revealed that the kidneys have the highest expression level of tsRNAs while the spleen had the lowest [Figure 3b]. However, the ratios of each subtype of tsRNAs within each tissue were comparable, with the bulk of expression being attributed to 3'tRFs followed by i-tRFs and tRF-1 [Figure 3c]. tiRNAs and 5'tRFs constituted a small fraction of the reads. Next, we examined the expression of 3'tRFs [Figure 3d], i-tRFs [Supplementary figure 4a], and tRF-1 [Supplementary figure 4b]. In all three subtypes, significant clustering patterns were observed between tissues as well as unique tsRNAs clusters enriched in various tissues were observed, with the kidney standing out with multiple unique tRFs clusters. Pearson's correlation across all three datasets revealed that most tissues had

moderate to excellent positive correlations [Figure 3e-g]. However, the spleen was standing out in all comparisons. All these data pointed out different clustering patterns compared to those observed at the levels of tRNA modifications and tRNA expression. This was confirmed when we conducted PLS-DA analysis using the entire tsRNAs dataset [Supplementary figure 5], which revealed a unique cluster for the kidneys as well as another cluster for the spleen and lung while the heart, brain, and liver clusters overlapped.

Given that unique clustering patterns were observed, we asked whether the expression of tsRNAs in different tissues is derived by certain motifs or lead to certain motif enrichments that can give clues as to the function of such tsRNAs. First, we started by analyzing the top 20 3'tRFs, i-tRFs, and tRF-1s, by normalized read counts, in all tissues. 3'tRFs showed enrichment of motifs containing TTCG in all tissues except the spleen, which had unique motifs [Figure 4]. Moreover, the lung and the brain also had unique motifs in their 3'tRFs that were not evident in other tissues. Analysis of i-tRF motifs revealed a different set of motif enrichment in all tissues, which can reflect functional differences between tsRNAs, and also, more motif sequence diversity as to what was observed in 3'tRFs [Supplementary figure 6]. Certain motif sequences were observed in more than one tissues, such as the motifs YWGGATTC in kidney and YWGRATTC in liver or TAGGATTC in both lungs and muscle which can reflect functional similarities between these tissues or common shared regulatory processes. tRF-1, on the other hand, had very strong motif sequence similarity between tissues, with TCGA sequence being present in all top motifs in all tissues [Supplementary figure 7].

- **Unique translational patterns observed in various tissues.**

To understand the impact of tRNA epitranscriptome on tissues specific translational

patterns, we conducted Ribosome profiling (Ribo-seq) on each tissue. We were mainly interested in observing the clustering patterns at the translational level as well as conducting codon analytics to corroborate these data with our observations at the tRNA level. We used various ways to cluster tissues at the translational level; heatmap clustering [Figure 5a, supplementary figure 8a], tSNE [Figure 5b], and Gene level UMAP [Figure 5c], all revealed unique clustering of the brain vs other tissues. It was also evident that the clustering patterns observed at the translational level could faithfully replicate those observed at the tRNA modifications level [Figures 1c and 1d], where the brain was somewhat unique but closer to kidneys and liver, while the spleen and lung clustered closely together as well as the heart and muscles. We next analyzed the differentially translated genes (DTGs) in each tissue versus all the others [Figure 5d] and observed various gene translational patterns. The brain showed the largest number of significant DTGs versus other tissues followed by the liver and heart. Indeed, this was also evident when we conducted detailed DTG analysis for tissue pairs [Supplementary table 3]. Using the DTGS from each tissue versus all others, we conducted gene ontology biological processes (GOBP) pathway analysis, which showed using clustering for each tissue in terms of enriched pathways, with significant overlaps between closely related tissues (Heart and muscle or lung and spleen) [Supplementary figure 8b]. In addition, the activation matrix of GOBP pathways showed unique pathway enrichment that also followed the clustering patterns of tissues. Moreover, pathways related to mitochondrial function and muscle contraction were enriched in the heart and muscles, in agreement with the enrichment of f5C and f5Cm modifications and Mt-tRNAs for example. Finally, we evaluated whether the clustering and gene translation patterns in different tissues can be used to accurately annotate such tissues [Supplementary figure 9]. We observed a large

degree of agreement between the annotated tissues and the actual tissues analyzed, indicating the robustness of our sequencing in mapping, and discriminating the tissues and their translational patterns. We further explored our Ribo-seq data for the expression of known tRNA and small RNA modifying enzymes, with a focus on tRNA-Q and mcm5U related enzymes(Suzuki, 2021) [Supplementary figure 10a]. While we observed differences in expression across tissues, clustering, enzyme expression, as well as PLS-DA analysis did not correlate with what we observed at the level of tRNA modifications themselves [Supplementary figure 10b], indicating that the changes observed at the modifications levels are not mainly driven by differences in enzyme expression between tissues.

- **Tissue codon usage and optimality is governed by tRNA modifications levels.**

  tRNA modifications are known to drive mRNA translation by altering codon recognition, usage, and optimality(Chan et al., 2012; Cirzi et al., 2023; Suzuki, 2021). To elucidate the potential for such regulatory fine-tuning on tissue specific mRNA translation, we analyzed three metrics for codon analysis; isoacceptors codon frequency (which measures the ratio of expression between codons belonging to the same amino acids, i.e., isoacceptors), total codon frequency (which measures the ratio of expression between each codon and all other codons, i.e., mRNA codon composition)(Rashad et al., 2022; Tumu et al., 2012), and A-site pausing (which measures the ribosome stalling at each codon)(Liu et al., 2020) [Supplementary figure 11].

  First, we started by analyzing the codon isoacceptors frequencies in each tissue using the top and bottom 200 expressed genes by normalized read counts [Figure 6]. Heatmap clustering revealed a distinctive A/T vs G/C ending codon bias with few exceptions [Figure 6a, supplementary figure 12a]. In addition, the liver, lung, kidney,

spleen, and muscle showed strong underusage of the G/C ending codons given the enrichment of such codons in the downregulated genes and relative underusage in the upregulated genes. On the other hand, the brain and heart were not strongly biased in that sense. Pearson's correlation coefficient analysis was done on the isoacceptors frequencies of the top and bottom 200 genes separately [Figure 6b]. It was evident that the differences in tissues were mainly apparent in the downregulated genes, with the brain being furthest from all tissues except the heart. Further, PLS-DA analysis revealed unique clustering patterns reminiscent of what was observed at the level of tRNA modifications and translation, with few exceptions. For example, the spleen and lung clustered together and were far from the brain [Figure 6c, supplementary figure 12b]. Based on the impression from our data that the brain is unique compared to other tissues, we focused our attention on 2 tRNA modifications clusters which were highly expressed in the brain; tRNA-Q and its derivatives mannosyl-queuosine (manQ) and galactosyl-queuosine (gal-Q) and the mcm5U cluster and its related modifications and their corresponding codons. First, we explored the usage of Q-decoded codons and their correlation with the expression of tRNA-Q [Figure 6d]. tRNA-Q decodes NAC codons(Huber et al., 2022), which includes Asn-AAC, Asp-GAC, His-CAC, and Tyr-TAC. manQ decodes Asp-GAC while galQ decodes Tyr-TAC. We observed a positive correlation between Q-codons and Q modifications, except for Tyr-TAC. It is notable that Q and manQ were enriched in the brain but galQ did not show such enrichment [Figure 1b]. In addition, Tyr-TAC did not show a strong bias in our analysis as compared to other Q-codons [Figure 6a]. Next, we analyzed the correlation between Q-codons and anticodons [Figure 6e], which revealed a weaker correlation that what was observed at the modifications level as well as some negative correlation. It is also notable to mention that the Q-codons,

NAC codons, were negatively correlated with their isoacceptors in our analysis, signifying strong codon bias and selection [Figure 6f]. On the other hand, for mcm5U and mcm5s2U modifications, which are considered to be related to NAA codons recognition, mcm5U showed a positive correlation trend with GlnCAA and LysAAA, while mcm5s2U showed a negative correlation trend with LysAAA [Figure 6g], and the correlation coefficient for the other NAA codons was generally low, compared to Q codon. mcm5U codons also did not show strong correlation with their anticodons [Figure 6h], however, the NAA and their isoacceptors were showing clear bias in their usage [Figure 6i]. To further elucidate these clustering patterns, we analyzed the Q and mcm5U codons correlation with all modifications and anticodons detected in our analysis [Supplementary figure 13]. Indeed, distinct clustering patterns at each level were observed for Q codons [Supplementary figure 13a-c], while mcm5U codons showed weaker clustering and paradoxical correlations in some instances [Supplementary figure 13d-f]. These clustering patterns signifies that not only the usage of these codons are driven by their modifications, but the global translational and epitranscriptional dynamics also plays important role in dictating codon usage and biases.

Next, we repeated our analysis at the level of total codon usage, which can give us clues as to the mRNA amino acids and sequence preferences [Figure 7]. In this analysis, we observed strong bias in all tissues between codon frequencies in the top and bottom expressed mRNAs [Figure 7a], but with weaker A/T vs G/C ending codon bias. Differences between tissues were apparent in the bottom 200 genes and not the top 200 genes when we conducted Pearson's correlation coefficient analysis [Figure 7b]. In addition, PLS-DA analysis, while the tissues showed different clustering patterns compared to isoacceptors frequencies, still showed the brain to be

unique while the lung and spleen clustered together [Figure 7c and supplementary figure 14]. The correlation between Q-codons and mcm5U-codons with their respective modifications or anticodons was weaker or disappeared altogether, and there was no bias observed between isoacceptors in their total codon frequencies counts [Figure 7d-i].

Finally, we examined the ribosomal A-site pausing, which gives an indicator of the speed of decoding and codon optimality [Figure 8]. Q-codons, except for Asp-GAC, were readily decoded in the brain compared to other tissues, indicating increased optimality [Figure 8a and b]. While mcm5U codons showed variable optimality, with NAA mcm5U codons being readily decoded, while Gly-GGA and Ala-GCA having variable optimality or being suboptimal altogether [Figure 8a and c]. Pearson's correlation coefficient between tissues using the A-site pausing revealed good positive correlation between all tissues, in terms of their comparison to the brain, except for the liver and lung, which had modest negative correlation [Figure 8d]. This can also be an indicator of the uniqueness of codon optimality in the brain versus all other tissues.

➢ Discussion

In this work we present a comprehensive analysis of the tRNA epitranscriptome and identify its role in regulating codon usage and optimality across tissues. Importantly, our work highlights tRNA modifications as master regulators of codon usage across tissues. While several previous works have attempted to tackle this subject from various angles(Guo et al., 2023; Pinkard et al., 2020; Yu et al., 2022), our work represents the first comprehensive analysis of the various layers of the tRNA epitranscriptome and their direct correlation to translatomes to the best of our knowledge.

At the tRNA modification levels, previous works by Guo et al(Guo et al., 2023) showed tissue specific enrichment levels but did not include the analysis of many modifications that are of great importance in fine-tuning codon optimality in tissues, such as tRNA queuosine. Further, previous works did not directly correlate tRNA epitranscriptome with codon decoding and translation(Guo et al., 2023; Pinkard et al., 2020) or used limited metrics for codon analysis(Yu et al., 2022). Here, we directly analyzed the impact of tRNA epitranscriptome on mRNA translation and codon decoding using multiple metrics. We observed that tRNA modifications play a critical and clear role in dictating codon optimality across tissues, thus positioning them as master regulators of tissue specific mRNA translation. We also observed that tRNA modifications impacted codon usage and bias on two metrics: isoacceptors frequencies, and ribosome A-site pausing, both of which reflects codon bias and optimality. However, such strong correlation between modifications and codons was significantly diminished when total codon frequencies were considered. Total codon frequencies reflect mRNA sequence preferences, and not codon bias per se. This observation could be attributed to the fact that the modifications focused on herein, queuosine and its derivatives and mcm5U and its derivatives, both regulate codon bias via impacting isoacceptors codons decoding fidelity(Endres et al., 2015; Suzuki, 2021; Tuorto et al., 2018).

tRNA modifications have been recognized as important players in many diseases and conditions(Dedon and Begley, 2022; Delaunay et al., 2022; Rosselló-Tortella et al., 2020). However, the cell-specific physiological roles are not explored for most known modifications. In our work, we identified tRNA queuosine to be preferentially enriched in the brain and drive NAC codon recognition. Queuosine modifications were shown to play important role in regulating cellular response to arsenite induced oxidative stress and mitochondrial dysfunction(Huber et al., 2022), as well as playing a role in hippocampal neurons function and cognition(Cirzi et al., 2023). Interestingly, despite the reported importance of queuosine in codon decoding *in vitro(Tuorto et al., 2018)*, Knockout mice were phenotypically normal apart from cognitive and memory dysfunction(Cirzi et al., 2023). In addition, the presence of a neural only phenotype indicates the importance of tRNA-Q in brain function, in line with previous works that showed that queuine, the precursor for queuosine, is protective against neurodegenerative diseases(Richard et al., 2021) and our observation of queuosine enrichment in the brain. This neural-specific phenotype sheds light as well on tissue and cell specific physiological functions of tRNA modifications that are rarely addressed. In the case of queuosine, it appears that the enrichment in the brain is vital for proper neuronal functioning, evident by Cirzi et al work(Cirzi et al., 2023). Such observations highlight the importance of understanding cell and tissue specific dependencies on tRNA modifications for proper translation in understanding tissue development, physiology, and pathologies.

Another important observation in our work was the significant enrichment of f5C and f5Cm in the heart and muscles, two modifications with reported links to mitochondrial function(Delaunay et al., 2022; Kawarada et al., 2017). The heart and muscles, also, have higher mitochondrial content that other tissues(Fernandez-Vizarra et al., 2011). This correlation brings about an interesting possibility of using f5C and f5Cm tRNA levels as

biomarkers for mitochondrial content and bioenergetics at the tissue and cell levels. We also observed an interesting trend of enrichment of a cluster of modifications in the spleen, namely m6A, m6Am, m227G, and 2'O-ribose methylations. m6A, m6Am, and m227G were not described previously in the tRNA(Suzuki, 2021), but do exist in other RNAs that co-elute in the small RNA fractions extracted. Further, this cluster of modifications was also enriched in the lung, making a compelling case of immune linked function of these modifications(Ardain et al., 2020). It is notable to mention that other modifications, such as m1A, were reported to play important roles in immune cell function(Liu et al., 2022b). m1A was also enriched in the lungs as well as the heart followed by the spleen, in agreement with these notions. Indeed, both the lung and spleen had lower tRNA levels and higher snRNA and other small non-coding RNA levels (such as rsRNAs)(Shi et al., 2021). This opens the possibility of using small RNA modifications levels as a probe for the relative content of various small non-coding RNAs in various tissues and cell types in physiology and pathology. It is imperative to note that methods that isolate only mature tRNA for analysis would not capture such phenomena, which highlights the importance of various steps in the analytical process of RNA modifications in shaping the final results and conclusions. It is notable that many of the observed modifications are not studied in tissue or cell specific physiologic or pathologic contexts, and thus we cannot extrapolate our findings further. Another interesting observation was the near uniformity of tRNA isoacceptors (anticodon) expression across tissues, which was previously reported(Pinkard et al., 2020). While it was shown previously by Pinkard et al(Pinkard et al., 2020) that there are tissue specific isodecoder tRNA level differences, tRNA isoacceptors expression were very stable across tissues. This agreement between our work and Pinkard et al(Pinkard et al., 2020) work despite using very different tRNA sequencing techniques validates their data greatly, as well as ours. Importantly, while tRNA isoacceptors were shown to dynamically change in

pathologies such as oxidative stress(Torrent et al., 2018) and cancer(Goodarzi et al., 2016) to impact codon decoding, it appears that this role is more or less stable in physiology. This also highlights the role of tRNA modifications as the main regulator of codon usage and optimality in physiological states across tissues and cells.

While our analysis focused heavily on tRNA modifications and their impact on codon optimality, we were also able to extract information on tsRNAs, which play important epitranscriptional roles and have been recognized as regulators of many diseases and processes(Kuhle et al., 2023; Rashad et al., 2020b). Here, we were interested in the expression of different tsRNAs in various tissues and also what regulates such expression. We observed various tissue specific enrichment patterns in multiple tRF subtypes. Importantly, we report for the first-time tissue specific motif enrichment in multiple tRF subtypes that was not previously reported to the best of our knowledge. Such motif enrichment was observed previously to regulate microRNA export via extracellular vesicles(Garcia-Martin et al., 2022). Indeed, tRFs are known to exist in the blood and to be exported from cells(Li et al., 2022). In our analysis, we identified tRF subtype specific motifs. We also identified that different tRFs show different patterns of motif sequence diversity between tissues. While i-tRF showed strong motif diversity between tissues, tRF-1, which is generated from pre-tRNAs(Zhang et al., 2020), exhibited strong motif similarity. tRFs were previously shown to interact with ribosomes and proteins as well as acting via microRNA-like mechanisms to regulate translation(Gong et al., 2023). Whether such the discovered tRFs motifs play a role in their functions, such as in regulating their export or interaction with proteins, remain to be explored.

Codon usage and optimality have been a subject of immense interest, given their role in regulating many molecular processes such as mRNA stability and decay(Bae and Coller, 2022; Presnyak et al., 2015), ribosome decoding fidelity(Buschauer et al., 2020), and mRNA

translation efficiency(Hanson and Coller, 2018; Nedialkova and Leidel, 2015). Previous works revealed a plasticity of codon optimality that adapts to cell states. For example, during oxidative stress, tRNA modifications and tRNA expression dynamically change to alter codon optimality and drive translation of antioxidant proteins(Huber et al., 2022; Torrent et al., 2018). This also occurs during cell proliferation and differentiation(Bornelov et al., 2019; Guimaraes et al., 2020). Such findings made it more likely that tissue-specific codon optimality can regulate mRNA translation and local proteostasis. Such idea was challenged previously in Drosophila tissues by Allen et al(Allen et al., 2022). In their work, Allen et al(Allen et al., 2022) used codon mutated probes to evaluate the expression of rare codons in various tissues. In their work, they found that the testis and brain are capable of expressing rare codons compared to other tissues. Attempts to elucidate tissue-specific codon optimality in mammalian tissues have been limited to date, and mostly relied on published datasets(Sun and Zhang, 2022) and public databases(Benisty et al., 2023), thus the analysis was usually limited by the data available. For example, no formal correlation between tRNA pools or tRNA modifications was made to explain codon optimality patterns or specific phenomena observed at the codon level in such published works(Benisty et al., 2023; Sun and Zhang, 2022), especially that the reliance on tRNA genes does not reflect actual tRNA transcript expression(Chan and Lowe, 2016). In addition, the reliance on codon adaptation index (CAI) or tRNA adaptation index (tAI) might also not be ideal in such contexts where tissue specific metrics are needed, given that these two metrics depend on genomic information and not actual mRNA or tRNA levels(Sabi et al., 2017; Sharp and Li, 1987). This work presented herein represents the first analysis of mammalian codon usage and optimality that relies on tissue specific translational levels to deduce codon optimality. While many important works have shown the role of tRNA modifications in regulating codon optimality and the decoding fidelity of ribosomes(Chan et al., 2012; Nedialkova and Leidel, 2015; Rossello-Tortella et al.,

2020; Suzuki, 2021; Tuorto et al., 2018), this work represents evidence of such regulation at the tissue level in mammals. Our work, supported by previous work from Pinkard et al(Pinkard et al., 2020), also shows that actual tRNA transcript expression does not appear to play important roles in driving codon optimality, given the uniformity across tissues. In our work, we also show an important feature of the strong correlation between tRNA modifications and their decoded codons at the level of isoacceptors frequencies and A-site pausing, while this correlation weakens when we analyzed total codon frequencies across mRNAs. This further indicates that tRNA modifications drive mRNA translation via synonymous codon usage and bias.

Despite our best efforts to provide a comprehensive analysis of tRNA epitranscriptome and tissue-specific translatomes, there are certain limitations that should be taken into consideration when viewing this work. Firstly, the impact of tRNA modifications on tissue specific codon recognition needs further validation. While knockout mouse models for example can be used to systematically study such links, as done in previous works(Cirzi et al., 2023; Endres et al., 2015), there are many modifications that were not studied in cell specific context. Secondly, an issue that wasn't discussed herein is the potential role of tsRNAs motifs in regulating their function. However, we believe that this process should be addressed separately. Thirdly, we conducted our analysis using only male mice at a certain age, thus sex specific differences, which were reported previously to have an impact on small non-coding RNAs expression(Isakova et al., 2020), were not addressed. Nonetheless, we contended with such a limitation to focus our work on the correlation between tRNA epitranscriptome and codon usage and bias.

In summary, our study offers a comprehensive view of the tRNA epitranscriptome and translatome across various mouse tissues. The identification of tissue-specific modification patterns, their potential functional roles, and their impact on codon bias provide valuable

insights into the intricate regulatory mechanisms governing translation in response to environmental cues. These findings significantly contribute to our understanding of the complex interplay between tRNA modifications, tRNA pools, codon recognition, and translation efficiency in a tissue-specific context. Future works should aim to address the impact of sex and age on the reported phenomena as well as to try and replicate such findings in higher mammals or humans if possible.

Methods

Animals and sample collection, RNA isolation

Eight-week-old male C57BL/6J mice purchased from Kumagai Sigeyasu Shoten (Sendai, Japan) were maintained on a 12-hour light-dark cycle. For LC-MS/MS analysis, four mice were perfused with ice-cold PBS and tissues (brain, lung, heart, liver, spleen, kidney, and muscle) were extracted immediately after perfusion and flash-freeze until RNA extraction. Tissues were homogenized with QIAzol (QIAGEN, Hilden, Germany, catalog # 79306) and isolate small RNA using Purelink miRNA Isolation Kit (Thermo Fisher, catalog # K157001). For small RNA sequencing and Ribosome profiling, three mice were perfused using ice-cold phosphate buffered saline with 100 µg/ml cycloheximide (Sigma, MO, catalog # 01810). Tissues were extracted immediately after perfusion and flash-freeze until RNA extraction. Tissues were homogenized with lysis buffer (20 mM Tris-Cl pH 7.5, 150 mM NaCl, 5 mM MgCl2, 1 mM dithiothreitol (Sigma, catalog # D9779), 100 µg/ml Cycloheximide, and 1% Triton X-100) and centrifuge at 13000 x g at 4°C for 15 min. For small RNA sequencing, 100 µl of supernatants were transferred to fresh tubes, and then 900 µl of QIAzol was added. Subsequently, small RNA was isolated using Purelink miRNA Isolation Kit, according to the manufacture's protocol. For Ribosome profiling, 500 µl of supernatant was kept for downstream procedure. All animal experiments were conducted according to the procedures approved by the animal care facility of Tohoku University and according to the ARRIVE (Animal Research: Reporting In Vivo Experiments) guidelines. Ethical board approval was acquired prior to the commencement of this project.

Small RNA quality control

Nanodrop one was used to analyze RNA concentration and purity. RNA integrity was analyzed using Bioanalyzer 2100 and the Agilent bioanalyzer small RNA kit (Agilent, #5067-1548). Example bioanalyzer traces are provided in supplementary figure 2.

Quantitative analysis of tRNA modifications by Mass spectrometry

Quantitative liquid chromatography tandem mass spectrometry (LC-MS/MS) analysis of RNA modifications was done as reported previously with modifications(Su et al., 2014). Small RNA enriched RNA fractions, which contained around 90% mature tRNA, were digested for 6 hours at 37°C using a digestion mixture of: MgCl2 2.5mM, Tris (pH 8) 5mM, Coformycin 0.1µg/ml, deferoxamine 0.1mM, Butylated hydroxytoluene 0.1mM, Benzonase 0.25U/µl, Calf intestinal alkaline phosphatase (CIAP) 0.1U/µl, and Phosphodiesterase I (PDE I), 0.003U/µl. Samples and standards were injected into Waters BEH C18 column (50 × 2.1 mm, 1.7 µm) coupled to an Agilent 1290 HPLC system and an Agilent 6495 triple-quad mass spectrometer. The LC system was conducted at 25 °C and a flow rate of 0.3 mL/min. Buffer A was composed of 0.02% formic acid (FA) in DDW. Buffer B was composed of 0.02% FA in 70% Acetonitrile. The buffer gradient is shown in supplementary table 4. The UPLC column was coupled to an Agilent 6495 triple quad mass spectrometer with an electrospray ionization source in positive mode with the following parameters: gas temperature, 200 °C; gas flow, 11 L/min; nebulizer, 20 psi; sheath gas temperature, 300 °C; sheath gas flow, 12 L/min; capillary voltage, 3000 V; nozzle voltage. Dynamic MRM was used to detect modifications using transitions and collision energies listed in supplementary table 5. Peak areas were normalized to the sum of UV signal of the canonical nucleotides (U, C, G, and A) and expressed as area ration. Four biological replicates were used per group.

Small RNA sequencing

We used Arm-seq method as described previously(Cozen et al., 2015) with some modifications. Briefly, to remove 3' conjugated amino acids, 500 ng RNA sample was deacylated in 0.1 M pH 9.0 Tris-HCl buffer at 37°C for 1 hour. Deacylated RNA was treated with AlkB demethylase (rtStar tRNA-optimized First-Strand cDNA Synthesis Kit, ArrayStar, catalog # AS-FS-004) at ambient temperature for 2 hours to reduce tRNA methylation. RNA was purified using Zymo Directzol RNA micro kit (Zymo reserch, catalog # R2060) and end repaired with T4 Polynucleotide Kinase (T4 PNK; NEB, catalog # M0201) at 37°C for 30 min. All treated RNA samples were used for library preparation using NEBNext Multiplex Small RNA Library Prep Set for Illumina (NEB catalog # E7300/7580) according to the manufacturer protocol. Size selection of amplified cDNA library was performed using 6% TBE PAGE in a range of 140 to 210 bp (microRNA to mature tRNA). Library concentration and quality were assessed by Bioanalyzer 2100 using DNA 1000 chip (Agilent, #5067-1504). All the samples were pooled and sequenced by Illumina Hiseq-X ten instrument in a pair-end, 150 bp read. Three biological replicates were used per group.

Small RNA sequencing data analysis

Small RNA libraries were first processed by tRAX software(Li et al., 2022) to perform adaptor trimming and alignment to mouse tRNA reference (mm10 genome) as well as quality control. tRAX was used to analyze mature tRNA and anticodons expression. For tsRNAs, trimmed fastq files were analyzed using MINTmap software using MINTbase database reference(Pliatsika et al., 2016). tsRNAs were divided into tRNA halves (tiRNAs) and tRNA derived fragments (tRFs) as per naming conventions [Figure 3a]. tsRNAs reads were normalized to all the reads in each sample and the normalized reads were used for downstream analysis. Motif analysis was conducted on tRFs using Meme-suite(Bailey et al., 2015) with the parameters: ZOOPS, minimum width = 6, maximum width = 8, minimum sites = 2, and maximum number of motifs = 3.

Ribosome profiling

Ribosome profiling was performed as we previously reported(Zhou et al., 2023), which was based on another protocol with few modifications(Vu et al., 2017). Ribosome foot-printing was performed on samples collected as mentioned above by adding 1.25U/µl RNase I (NEB Catalog# M0243L) to 500µL clarified lysate and incubating samples on rotator mixer for 45min at room temperature. TRIzol reagent was added, and RNA extracted using Qiagen miRNeasy kit. Ribosome protected fragments (RPFs) were selected by isolating RNA fragments of 27-35 nucleotides (nt) using TBE-Urea gel. rRNA depletion was conducted using NEBNext rRNA depletion kit v2 (NEB, # E7400L) followed by end-repair using T4 PNK after purification of the rRNA depleted samples using zymo oligo clean and concentrator kit (Zymo research, # D4060). The preparation of sequencing libraries for ribosome profiling was conducted via the NEBNext Multiplex Small RNA Library Prep kit for Illumina according to the manufacturer's protocol (NEB, # E7300S). Pair-end sequencing reads of size 150bp were produced for Ribo-seq on the Ilumina Hiseq X-ten system. Three biological replicates were prepared per group.

Ribosome profiling data analysis

Quality control for Raw Fastq was performed using FastQC. Next, adapter trimming and collapsing the pair-end reads into one was done using Seqprep. Trimmomatic(Bolger et al., 2014) was used to further clean low quality reads. Bowtie2(Langmead and Salzberg, 2012) was used to align the reads to a reference of rRNA and tRNA genes (mm10) to remove contaminants. After that, reads were aligned to the genome (mm10 downloaded from UCSC), reads counted using FeatureCounts(Liao et al., 2014), and differential expression conducted using Limma(Ritchie et al., 2015). Omics playgroud(Akhmedov et al., 2020) was used for Ribo-seq data visualization and clustering as well as read normalization. Of note, we also used

Stringtie(Pertea et al., 2016) to generate TPKM normalized read counts which were comparable to the log2CPM generated from Omics Playground, thus we performed downstream analysis using the Omics playground output.

Codon analysis

Isoacceptors frequency and total codon frequency were analyzed as we previously reported(Rashad et al., 2022; Tumu et al., 2012). The amino acid normalized codon frequency is calculated as:

$$\text{frequency of codon } i \text{ in gene } j = \frac{\text{number of occurrences of codon } i \text{ in gene } j}{\sum_{i=1}^{n} \text{number of occurrences of isoacceptor}_{ij}}$$

where isoacceptors refers to the synonymous codons for the amino acid encoded by codon *i* and n refers to the number of isoacceptors for a given amino acid ($2 \leq n \leq 6$).

The total codon frequency is calculated as:

$$\text{Total frequency of codon } i \text{ in gene } j = \frac{\text{number of occurrences of codon } i \text{ in gene } j}{\sum_{i=1}^{n} \text{number of occurrences of codon } i \text{ in gene } j}$$

where n refers to the total number of codons used in the gene.

The t-statistic describing the codon frequency was calculated as:

$$\text{T-statistic for codon } i = \frac{x_i - \mu_i}{s_i/\sqrt{n}}$$

Where x_i refers to the mean frequency for codon *i* in the sample, μ_i refers to the mean frequency for codon *i* across the Mus musculus genome, s_i refers to the standard deviation of the frequency for codon *i* in the sample, and n refers to the sample size.

A-site pausing was calculated using Ribotoolkit(Liu et al., 2020) where the brain was compared to each tissue to deduce the relative ribosome pausing at each codon. Next, the output was converted into log2 fold change for representation.

Data visualization and statistical analysis

Heatmaps and clustering and Pearson's correlation analysis were conducted using Morpheus (https://software.broadinstitute.org/morpheus). Hierarchical clustering was performed using the "one minus Pearson correlation" metric and "average" as the linkage method. PLS-DA was conducted using the *R* language package mixOmics(Rohart et al., 2017). Z-score analysis was conducted in *R*. ANOVA with Turkey's post hoc analysis was conducted using SPSS v20 (IBM corp.).

Data availability

Raw sequencing data were deposited in the sequence read archive (small RNA-seq: PRJNA1003133. Ribo-seq: PRJNA1004093). All other data are presented in the supplementary files. Further data can be provided by the corresponding author upon reasonable request.

Funding: This project was funded by the Japan society for promotion of science grants number #23H02741 and #20KK0338 for Rashad.

Author contribution: Ando D: Sample collection and processing, sequencing libraries preparation, data analysis and interpretation, writing. **Rashad S:** Study conception and design, LC-MS analysis, Bioinformatics analysis, Data analysis and interpretation, writing, supervision, funding. **Begley TJ:** Codon algorithm development. **Endo H:** critically revised the manuscript. **Aoki M:** critically revised the manuscript. **Dedon PC:** LC-MS data interpretation. critically revised the manuscript. **Niizuma K:** critically revised the manuscript.

Conflict of interest: The authors report no conflict of interest regarding this work.

References

Akhmedov, M., Martinelli, A., Geiger, R., and Kwee, I. (2020). Omics Playground: a comprehensive self-service platform for visualization, analytics and exploration of Big Omics Data. NAR Genom Bioinform *2*, lqz019.

Allen, S.R., Stewart, R.K., Rogers, M., Ruiz, I.J., Cohen, E., Laederach, A., Counter, C.M., Sawyer, J.K., and Fox, D.T. (2022). Distinct responses to rare codons in select Drosophila tissues. Elife *11*.

Ardain, A., Marakalala, M.J., and Leslie, A. (2020). Tissue-resident innate immunity in the lung. Immunology *159*, 245-256.

Bae, H., and Coller, J. (2022). Codon optimality-mediated mRNA degradation: Linking translational elongation to mRNA stability. Mol Cell *82*, 1467-1476.

Bailey, T.L., Johnson, J., Grant, C.E., and Noble, W.S. (2015). The MEME Suite. Nucleic Acids Res *43*, W39-49.

Benisty, H., Hernandez-Alias, X., Weber, M., Anglada-Girotto, M., Mantica, F., Radusky, L., Senger, G., Calvet, F., Weghorn, D., Irimia, M.*, et al.* (2023). Genes enriched in A/T-ending codons are co-regulated and conserved across mammals. Cell Syst *14*, 312-323 e313.

Bolger, A.M., Lohse, M., and Usadel, B. (2014). Trimmomatic: a flexible trimmer for Illumina sequence data. Bioinformatics *30*, 2114-2120.

Bornelov, S., Selmi, T., Flad, S., Dietmann, S., and Frye, M. (2019). Codon usage optimization in pluripotent embryonic stem cells. Genome Biol *20*, 119.

Buschauer, R., Matsuo, Y., Sugiyama, T., Chen, Y.H., Alhusaini, N., Sweet, T., Ikeuchi, K., Cheng, J., Matsuki, Y., Nobuta, R.*, et al.* (2020). The Ccr4-Not complex monitors the translating ribosome for codon optimality. Science *368*.

Chan, C.T.Y., Pang, Y.L.J., Deng, W., Babu, I.R., Dyavaiah, M., Begley, T.J., and Dedon, P.C. (2012). Reprogramming of tRNA modifications controls the oxidative stress response by codon-biased translation of proteins. Nature Communications *3*, 937.

Chan, P.P., and Lowe, T.M. (2016). GtRNAdb 2.0: an expanded database of transfer RNA genes identified in complete and draft genomes. Nucleic Acids Res *44*, D184-189.

Cirzi, C., Dyckow, J., Legrand, C., Schott, J., Guo, W., Perez Hernandez, D., Hisaoka, M., Parlato, R., Pitzer, C., van der Hoeven, F.*, et al.* (2023). Queuosine-tRNA promotes sex-dependent learning and memory formation by maintaining codon-biased translation elongation speed. EMBO J *42*, e112507.

Cozen, A.E., Quartley, E., Holmes, A.D., Hrabeta-Robinson, E., Phizicky, E.M., and Lowe, T.M. (2015). ARM-seq: AlkB-facilitated RNA methylation sequencing reveals a complex landscape of modified tRNA fragments. Nat Methods *12*, 879-884.

Crick, F.H. (1966). Codon--anticodon pairing: the wobble hypothesis. J Mol Biol *19*, 548-555.

Dedon, P.C., and Begley, T.J. (2022). Dysfunctional tRNA reprogramming and codon-biased translation in cancer. Trends Mol Med *28*, 964-978.

Delaunay, S., Pascual, G., Feng, B., Klann, K., Behm, M., Hotz-Wagenblatt, A., Richter, K., Zaoui, K., Herpel, E., Munch, C.*, et al.* (2022). Mitochondrial RNA modifications shape metabolic plasticity in metastasis. Nature *607*, 593-603.

Deng, W., Babu, I.R., Su, D., Yin, S., Begley, T.J., and Dedon, P.C. (2015). Trm9-Catalyzed tRNA Modifications Regulate Global Protein Expression by Codon-Biased Translation. PLoS Genet *11*, e1005706.

Endres, L., Begley, U., Clark, R., Gu, C., Dziergowska, A., Małkiewicz, A., Melendez, J.A., Dedon, P.C., and Begley, T.J. (2015). Alkbh8 Regulates Selenocysteine-Protein Expression to Protect against Reactive Oxygen Species Damage. PLoS One *10*, e0131335.

Fernandez-Vizarra, E., Enriquez, J.A., Perez-Martos, A., Montoya, J., and Fernandez-Silva, P. (2011). Tissue-specific differences in mitochondrial activity and biogenesis. Mitochondrion *11*, 207-213.

Garcia-Martin, R., Wang, G., Brandao, B.B., Zanotto, T.M., Shah, S., Kumar Patel, S., Schilling, B., and Kahn, C.R. (2022). MicroRNA sequence codes for small extracellular vesicle release and cellular retention. Nature *601*, 446-451.

Gong, M., Deng, Y., Xiang, Y., and Ye, D. (2023). The role and mechanism of action of tRNA-derived fragments in the diagnosis and treatment of malignant tumors. Cell Commun Signal *21*, 62.
Goodarzi, H., Nguyen, H.C.B., Zhang, S., Dill, B.D., Molina, H., and Tavazoie, S.F. (2016). Modulated Expression of Specific tRNAs Drives Gene Expression and Cancer Progression. Cell *165*, 1416-1427.
Guimaraes, J.C., Mittal, N., Gnann, A., Jedlinski, D., Riba, A., Buczak, K., Schmidt, A., and Zavolan, M. (2020). A rare codon-based translational program of cell proliferation. Genome Biol *21*, 44.
Guo, H., Xia, L., Wang, W., Xu, W., Shen, X., Wu, X., He, T., Jiang, X., Xu, Y., Zhao, P.*, et al.* (2023). Hypoxia induces alterations in tRNA modifications involved in translational control. BMC Biol *21*, 39.
Hanson, G., and Coller, J. (2018). Codon optimality, bias and usage in translation and mRNA decay. Nat Rev Mol Cell Biol *19*, 20-30.
Huber, S.M., Begley, U., Sarkar, A., Gasperi, W., Davis, E.T., Surampudi, V., Lee, M., Melendez, J.A., Dedon, P.C., and Begley, T.J. (2022). Arsenite toxicity is regulated by queuine availability and oxidation-induced reprogramming of the human tRNA epitranscriptome. Proc Natl Acad Sci U S A *119*, e2123529119.
Isakova, A., Fehlmann, T., Keller, A., and Quake, S.R. (2020). A mouse tissue atlas of small noncoding RNA. Proc Natl Acad Sci U S A *117*, 25634-25645.
Kawarada, L., Suzuki, T., Ohira, T., Hirata, S., Miyauchi, K., and Suzuki, T. (2017). ALKBH1 is an RNA dioxygenase responsible for cytoplasmic and mitochondrial tRNA modifications. Nucleic Acids Res *45*, 7401-7415.
Kuhle, B., Chen, Q., and Schimmel, P. (2023). tRNA renovatio: Rebirth through fragmentation. Mol Cell.
Langmead, B., and Salzberg, S.L. (2012). Fast gapped-read alignment with Bowtie 2. Nat Methods *9*, 357-359.
Li, G., Manning, A.C., Bagi, A., Yang, X., Gokulnath, P., Spanos, M., Howard, J., Chan, P.P., Sweeney, T., Kitchen, R.*, et al.* (2022). Distinct Stress-Dependent Signatures of Cellular and Extracellular tRNA-Derived Small RNAs. Adv Sci (Weinh) *9*, e2200829.
Liao, Y., Smyth, G.K., and Shi, W. (2014). featureCounts: an efficient general purpose program for assigning sequence reads to genomic features. Bioinformatics *30*, 923-930.
Liu, Q., Shvarts, T., Sliz, P., and Gregory, R.I. (2020). RiboToolkit: an integrated platform for analysis and annotation of ribosome profiling data to decode mRNA translation at codon resolution. Nucleic Acids Res *48*, W218-W229.
Liu, X., Mei, W., Padmanaban, V., Alwaseem, H., Molina, H., Passarelli, M.C., Tavora, B., and Tavazoie, S.F. (2022a). A pro-metastatic tRNA fragment drives Nucleolin oligomerization and stabilization of its bound metabolic mRNAs. Mol Cell *82*, 2604-2617 e2608.
Liu, Y., Zhou, J., Li, X., Zhang, X., Shi, J., Wang, X., Li, H., Miao, S., Chen, H., He, X.*, et al.* (2022b). tRNA-m(1)A modification promotes T cell expansion via efficient MYC protein synthesis. Nat Immunol *23*, 1433-1444.
Mao, Y., Dong, L., Liu, X.-M., Guo, J., Ma, H., Shen, B., and Qian, S.-B. (2019). m6A in mRNA coding regions promotes translation via the RNA helicase-containing YTHDC2. Nature Communications *10*, 5332.
Matsumura, Y., Wei, F.Y., and Sakai, J. (2023). Epitranscriptomics in metabolic disease. Nat Metab *5*, 370-384.
Mauger, D.M., Cabral, B.J., Presnyak, V., Su, S.V., Reid, D.W., Goodman, B., Link, K., Khatwani, N., Reynders, J., Moore, M.J.*, et al.* (2019). mRNA structure regulates protein expression through changes in functional half-life. Proc Natl Acad Sci U S A *116*, 24075-24083.
Murphy, F.V.t., and Ramakrishnan, V. (2004). Structure of a purine-purine wobble base pair in the decoding center of the ribosome. Nat Struct Mol Biol *11*, 1251-1252.
Nedialkova, D.D., and Leidel, S.A. (2015). Optimization of Codon Translation Rates via tRNA Modifications Maintains Proteome Integrity. Cell *161*, 1606-1618.
Oerum, S., Meynier, V., Catala, M., and Tisne, C. (2021). A comprehensive review of m6A/m6Am RNA methyltransferase structures. Nucleic Acids Res *49*, 7239-7255.

Pertea, M., Kim, D., Pertea, G.M., Leek, J.T., and Salzberg, S.L. (2016). Transcript-level expression analysis of RNA-seq experiments with HISAT, StringTie and Ballgown. Nat Protoc *11*, 1650-1667.
Pinkard, O., McFarland, S., Sweet, T., and Coller, J. (2020). Quantitative tRNA-sequencing uncovers metazoan tissue-specific tRNA regulation. Nat Commun *11*, 4104.
Pliatsika, V., Loher, P., Telonis, A.G., and Rigoutsos, I. (2016). MINTbase: a framework for the interactive exploration of mitochondrial and nuclear tRNA fragments. Bioinformatics *32*, 2481-2489.
Presnyak, V., Alhusaini, N., Chen, Y.H., Martin, S., Morris, N., Kline, N., Olson, S., Weinberg, D., Baker, K.E., Graveley, B.R.*, et al.* (2015). Codon optimality is a major determinant of mRNA stability. Cell *160*, 1111-1124.
Rashad, S., Byrne, S.R., Saigusa, D., Xiang, J., Zhou, Y., Zhang, L., Begley, T.J., Tominaga, T., and Niizuma, K. (2022). Codon Usage and mRNA Stability are Translational Determinants of Cellular Response to Canonical Ferroptosis Inducers. Neuroscience *501*, 103-130.
Rashad, S., Han, X., Sato, K., Mishima, E., Abe, T., Tominaga, T., and Niizuma, K. (2020a). The stress specific impact of ALKBH1 on tRNA cleavage and tiRNA generation. RNA Biol *17*, 1092-1103.
Rashad, S., Niizuma, K., and Tominaga, T. (2020b). tRNA cleavage: a new insight. Neural Regen Res *15*, 47-52.
Rashad, S., Tominaga, T., and Niizuma, K. (2021). The cell and stress-specific canonical and noncanonical tRNA cleavage. J Cell Physiol *236*, 3710-3724.
Richard, P., Kozlowski, L., Guillorit, H., Garnier, P., McKnight, N.C., Danchin, A., and Maniere, X. (2021). Queuine, a bacterial-derived hypermodified nucleobase, shows protection in in vitro models of neurodegeneration. PLoS One *16*, e0253216.
Ritchie, M.E., Phipson, B., Wu, D., Hu, Y., Law, C.W., Shi, W., and Smyth, G.K. (2015). limma powers differential expression analyses for RNA-sequencing and microarray studies. Nucleic Acids Res *43*, e47.
Rohart, F., Gautier, B., Singh, A., and KA, L.C. (2017). mixOmics: An R package for 'omics feature selection and multiple data integration. PLoS Comput Biol *13*, e1005752.
Rossello-Tortella, M., Llinas-Arias, P., Sakaguchi, Y., Miyauchi, K., Davalos, V., Setien, F., Calleja-Cervantes, M.E., Pineyro, D., Martinez-Gomez, J., Guil, S.*, et al.* (2020). Epigenetic loss of the transfer RNA-modifying enzyme TYW2 induces ribosome frameshifts in colon cancer. Proc Natl Acad Sci U S A *117*, 20785-20793.
Rosselló-Tortella, M., Llinàs-Arias, P., Sakaguchi, Y., Miyauchi, K., Davalos, V., Setien, F., Calleja-Cervantes, M.E., Piñeyro, D., Martínez-Gómez, J., Guil, S.*, et al.* (2020). Epigenetic loss of the transfer RNA-modifying enzyme TYW2 induces ribosome frameshifts in colon cancer. Proc Natl Acad Sci U S A *117*, 20785-20793.
Sabi, R., Volvovitch Daniel, R., and Tuller, T. (2017). stAIcalc: tRNA adaptation index calculator based on species-specific weights. Bioinformatics *33*, 589-591.
Sharma, S., Hartmann, J.D., Watzinger, P., Klepper, A., Peifer, C., Kotter, P., Lafontaine, D.L.J., and Entian, K.D. (2018). A single N(1)-methyladenosine on the large ribosomal subunit rRNA impacts locally its structure and the translation of key metabolic enzymes. Sci Rep *8*, 11904.
Sharp, P.M., and Li, W.H. (1987). The codon Adaptation Index--a measure of directional synonymous codon usage bias, and its potential applications. Nucleic Acids Res *15*, 1281-1295.
Shi, J., Zhang, Y., Tan, D., Zhang, X., Yan, M., Zhang, Y., Franklin, R., Shahbazi, M., Mackinlay, K., Liu, S.*, et al.* (2021). PANDORA-seq expands the repertoire of regulatory small RNAs by overcoming RNA modifications. Nat Cell Biol *23*, 424-436.
Su, D., Chan, C.T., Gu, C., Lim, K.S., Chionh, Y.H., McBee, M.E., Russell, B.S., Babu, I.R., Begley, T.J., and Dedon, P.C. (2014). Quantitative analysis of ribonucleoside modifications in tRNA by HPLC-coupled mass spectrometry. Nat Protoc *9*, 828-841.
Sun, M., and Zhang, J. (2022). Preferred synonymous codons are translated more accurately: Proteomic evidence, among-species variation, and mechanistic basis. Sci Adv *8*, eabl9812.
Suzuki, T. (2021). The expanding world of tRNA modifications and their disease relevance. Nat Rev Mol Cell Biol *22*, 375-392.

Torrent, M., Chalancon, G., de Groot, N.S., Wuster, A., and Madan Babu, M. (2018). Cells alter their tRNA abundance to selectively regulate protein synthesis during stress conditions. Sci Signal *11*.
Tumu, S., Patil, A., Towns, W., Dyavaiah, M., and Begley, T.J. (2012). The gene-specific codon counting database: a genome-based catalog of one-, two-, three-, four- and five-codon combinations present in Saccharomyces cerevisiae genes. Database *2012*.
Tuorto, F., Legrand, C., Cirzi, C., Federico, G., Liebers, R., Muller, M., Ehrenhofer-Murray, A.E., Dittmar, G., Grone, H.J., and Lyko, F. (2018). Queuosine-modified tRNAs confer nutritional control of protein translation. EMBO J *37*.
van den Born, E., Vagbo, C.B., Songe-Moller, L., Leihne, V., Lien, G.F., Leszczynska, G., Malkiewicz, A., Krokan, H.E., Kirpekar, F., Klungland, A.*, et al.* (2011). ALKBH8-mediated formation of a novel diastereomeric pair of wobble nucleosides in mammalian tRNA. Nat Commun *2*, 172.
Vu, L.P., Pickering, B.F., Cheng, Y., Zaccara, S., Nguyen, D., Minuesa, G., Chou, T., Chow, A., Saletore, Y., MacKay, M.*, et al.* (2017). The N(6)-methyladenosine (m(6)A)-forming enzyme METTL3 controls myeloid differentiation of normal hematopoietic and leukemia cells. Nat Med *23*, 1369-1376.
Yu, P., Zhou, S., Gao, Y., Liang, Y., Guo, W., Wang, D.O., Ding, S., Lin, S., Wang, J., and Cun, Y. (2022). Dynamic landscapes of tRNA transcriptomes and translatomes in diverse mouse tissues. Genomics Proteomics Bioinformatics.
Zhang, Y., Qian, H., He, J., and Gao, W. (2020). Mechanisms of tRNA-derived fragments and tRNA halves in cancer treatment resistance. Biomark Res *8*, 52.
Zhou, Y., Rashad, S., Tominaga, T., and Niizuma, K. (2023). Dynamic mRNA stability changes buffer transcriptional activation during neuronal differentiation and are regulated by RNA binding proteins. bioRxiv, 2023.2009.2022.558981.
Zuko, A., Mallik, M., Thompson, R., Spaulding, E.L., Wienand, A.R., Been, M., Tadenev, A.L.D., van Bakel, N., Sijlmans, C., Santos, L.A.*, et al.* (2021). tRNA overexpression rescues peripheral neuropathy caused by mutations in tRNA synthetase. Science *373*, 1161-1166.

Figure legends:

Figure 1: Analysis of tRNA modifications landscape across tissues. a: Schematic showing the tissues analyzed and methods used in this study. b: Expression of 45 different modifications across the 7 tissues. c: Pearson's correlation between different tissues. d: PLS-DA analysis of tissue clustering patterns. e: Pearson's correlation across modifications.

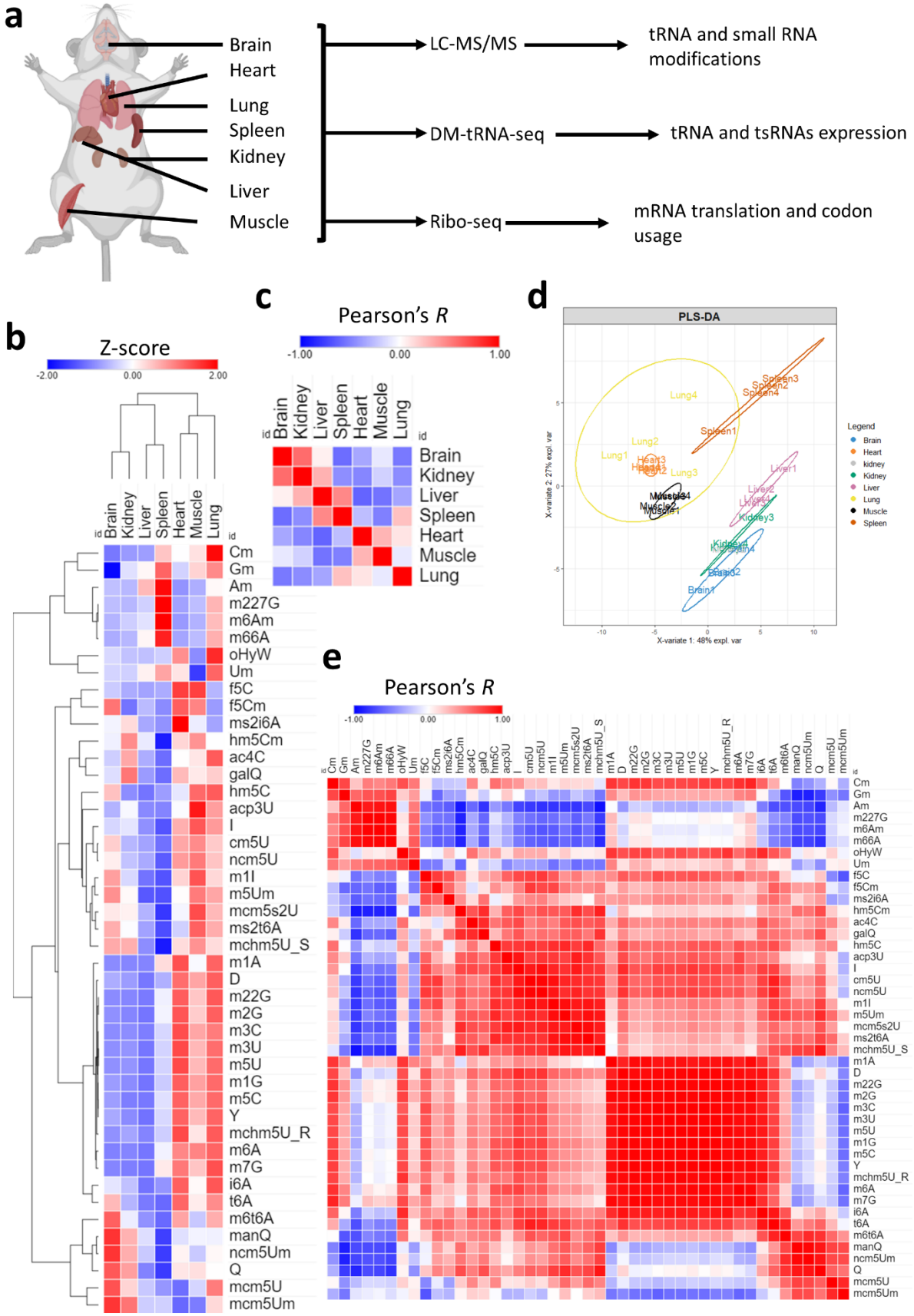

Figure 2: Analysis of mature tRNA expression across tissues. a: Distribution of detected small non-coding RNAs in our sequencing. b: Distribution of different amino acids representing tRNAs in the dataset. c: Expression of different mature tRNAs in our dataset normalized by their normalized read counts and represented as Z-score. d: Z-scores of mature tRNA expression across different tissues. e: Pearson's correlation coefficient between tissues based on Figure 2d. f: Pearson's correlation coefficient analysis between tissues based on figure 2c.

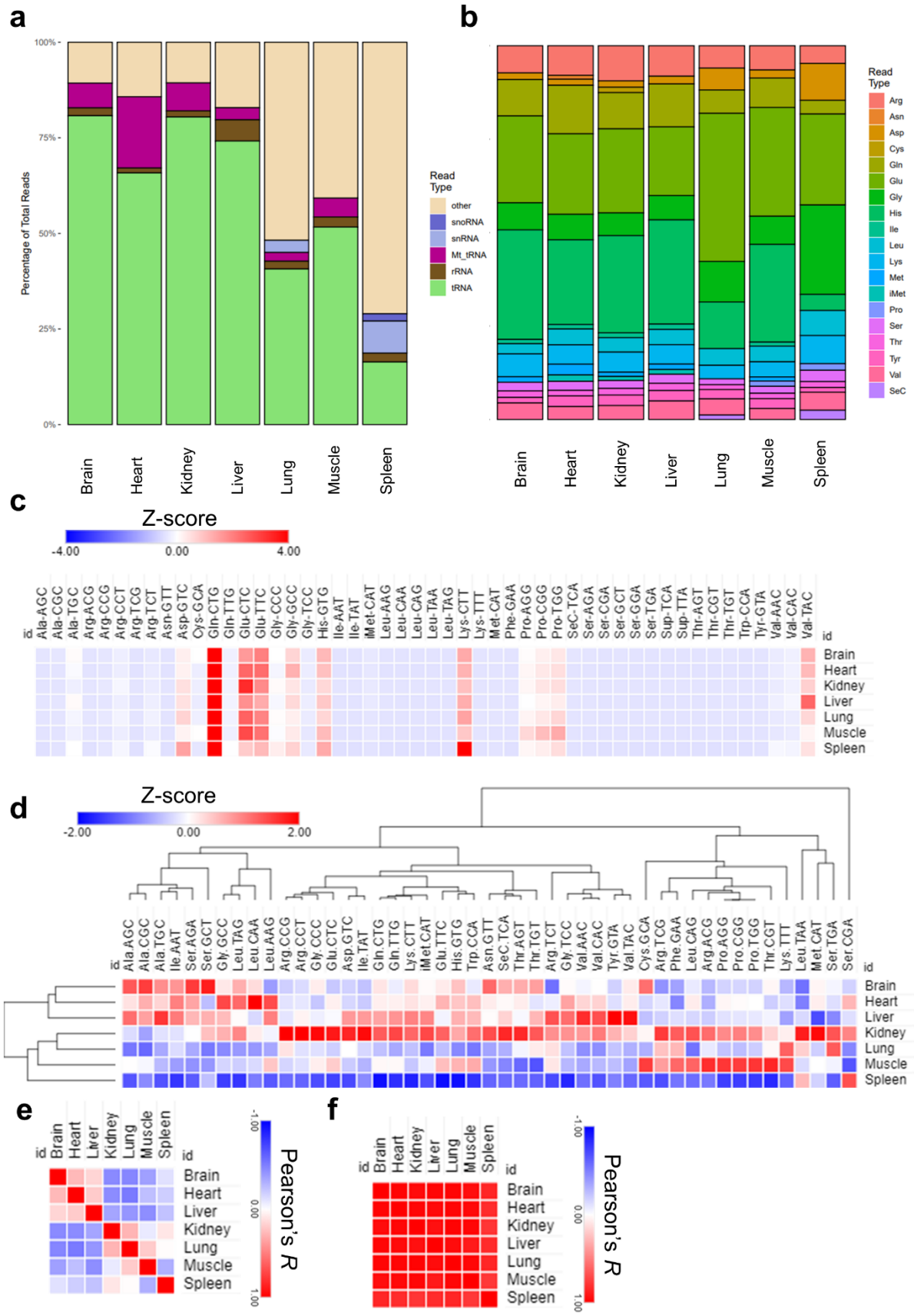

Figure 3: Analysis of tRNA derived small non-coding RNAs (tsRNAs) in different tissues. a: Schematic of different tsRNAs detected in our analysis. b: tsRNAs detected expression in each tissue represented as normalized read counts. c: Distribution of different tsRNAs in each tissue. d: Heatmap of 3'tRF expression. e: Pearson's correlation analysis between tissues using 3'tRFs as input. f: Pearson's correlation analysis using i-tRF expression. g: Pearson's correlation analysis using tRF-1 expression.

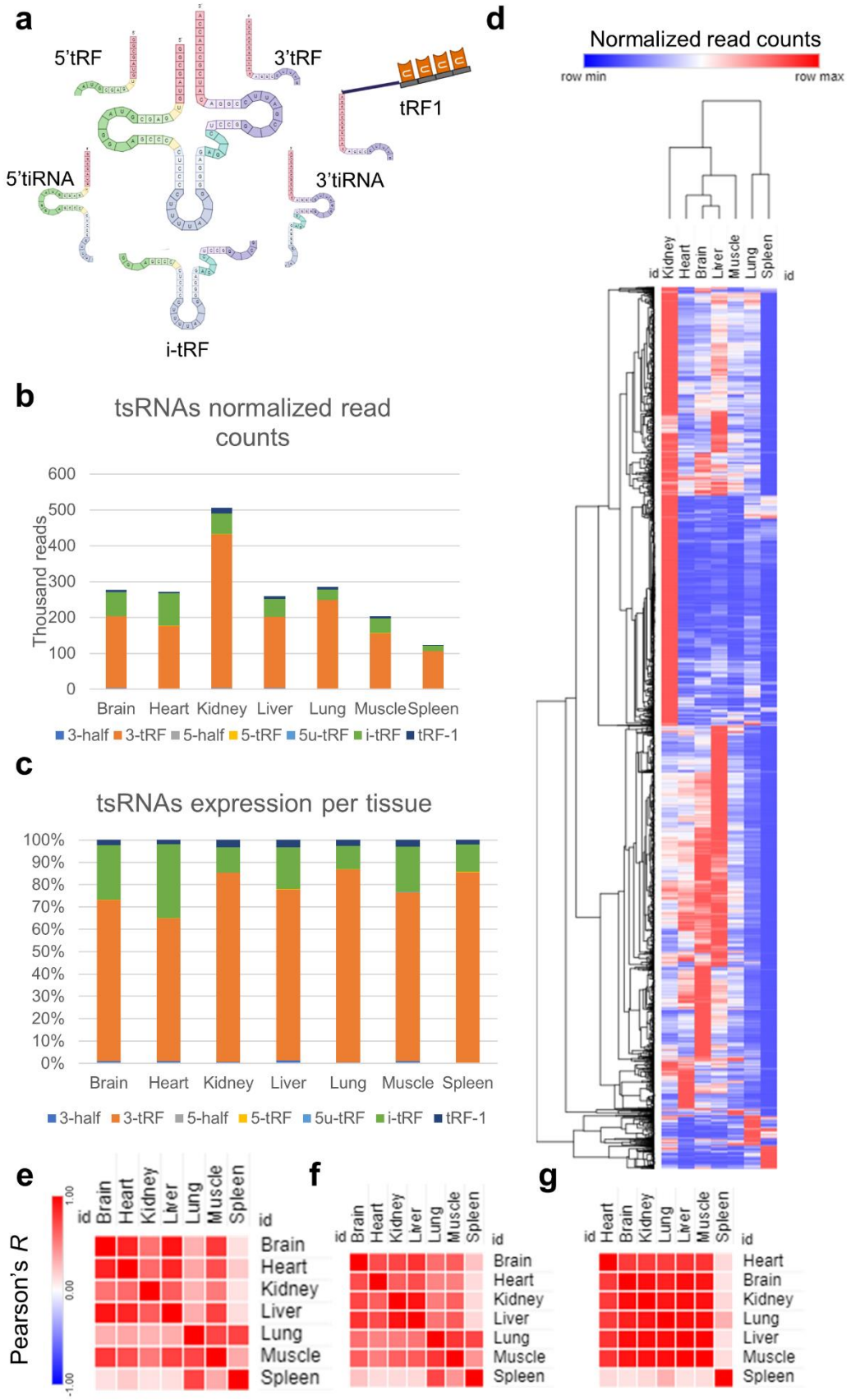

Figure 4: Motif analysis using top 20 expressed 3'tRFs from each tissue as input.

Tissue	Motif	Regular expression	Logo	E-value
Brain	GTTCGAHT	GTTC[GA]A[ACT]T		9.7e-033
	RSGARCC	[GA][CG]GA[AG]CC		3.5e-004
Heart	TTCGANTC	TTCGA[CTA]TC		3.2e-035
Kidney	TTCGARYC	TTCGA[GA][TC]C		1.9e-034
Liver	GTTCGAHT	GTTCGA[CAT]T		1.9e-029
Lung	TTCGADYC	TTCGA[ATG][TC]C		7.6e-036
	AGGGWCC	A[GA]G[GC][AT][CA][CG]		6.2e-004
Muscle	GTTCGAWT	GTTCGA[ATC]T		7.1e-035
Spleen	TCGAACCC	TCGAA[CA]CC		1.3e-036
	TCCCMGKB	T[CT]CC[CA][GC][TG][GTC]		3.9e-003

Figure 5: Ribo-seq analysis of tissue specific translational patterns. a: Heatmap clustering between tissues (Cluster annotation is in Supplementary figure 8a). b: Gene-level UMAP analysis. c: tSNE clustering analysis. d: Differentially translated genes (DTGs) analysis for each tissue versus all other tissues. e: Activation matrix of pathway enrichment using input from **d** at the GOBP level.

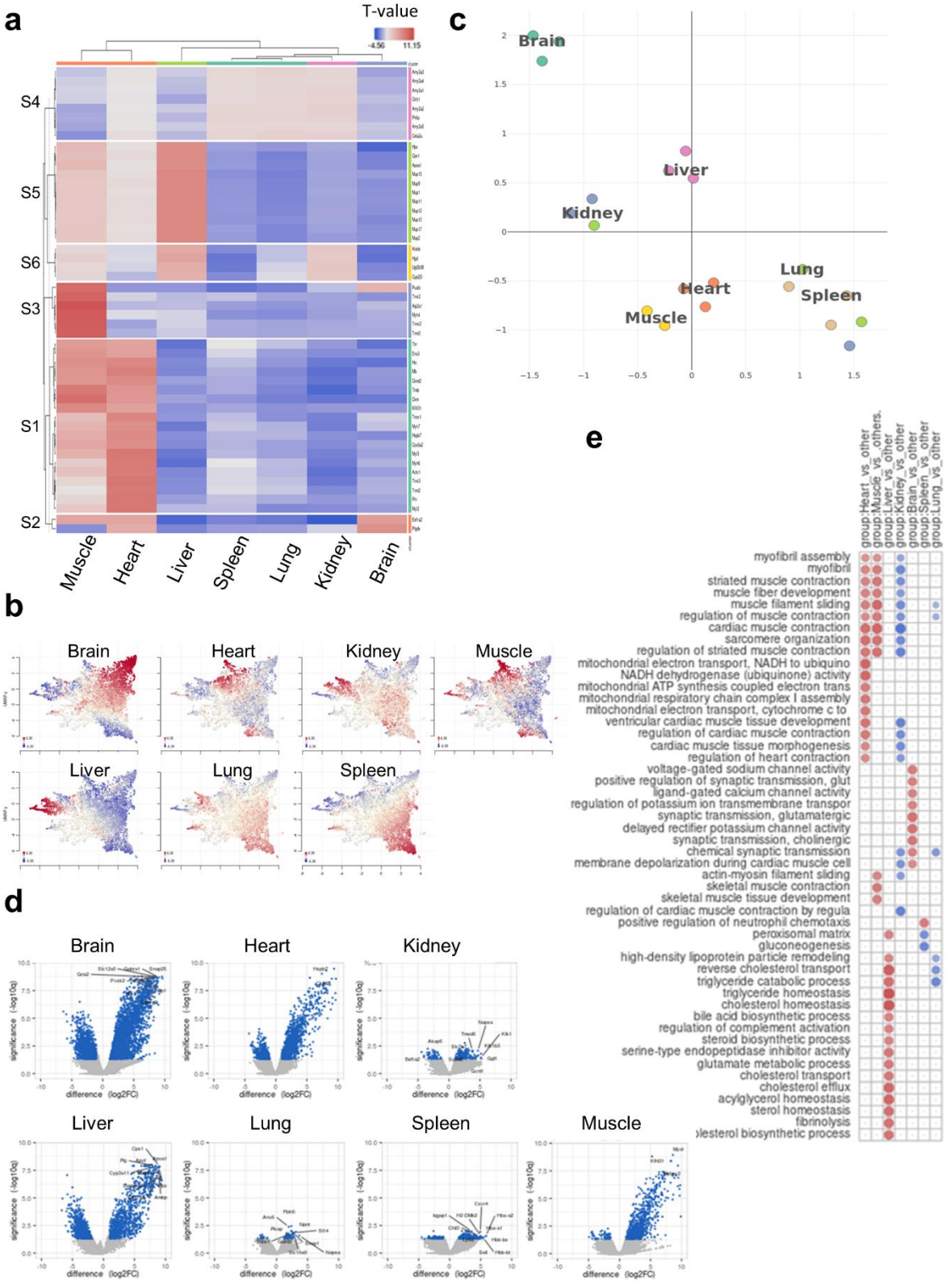

Figure 6: Analysis of isoacceptors codon usage. a: Heatmap of codon frequency in each tissue. Isoacceptors frequencies T-stats were calculated using top 200 counted genes (up) or bottom 200 genes (down) in each tissue. b: Heatmap of Pearson's correlation coefficients among 7 tissues by codon frequency from top (left) and bottom (right) 200 genes. c: PLS-DA analysis of tissue clustering patterns using the top 200 genes. d, e: Pearson's correlation analysis of codon frequency and Q modification enrichment (d) or Q related anticodons (e). f: Pairwise correlation analysis of Q codon from figure 6a. g, h: Pearson's correlation analysis of codon frequency and mcm5U and similar modification enrichment (g) or mcm5U related anticodons (h). i: Pairwise correlation analysis of mcm5U codon from figure 6a.

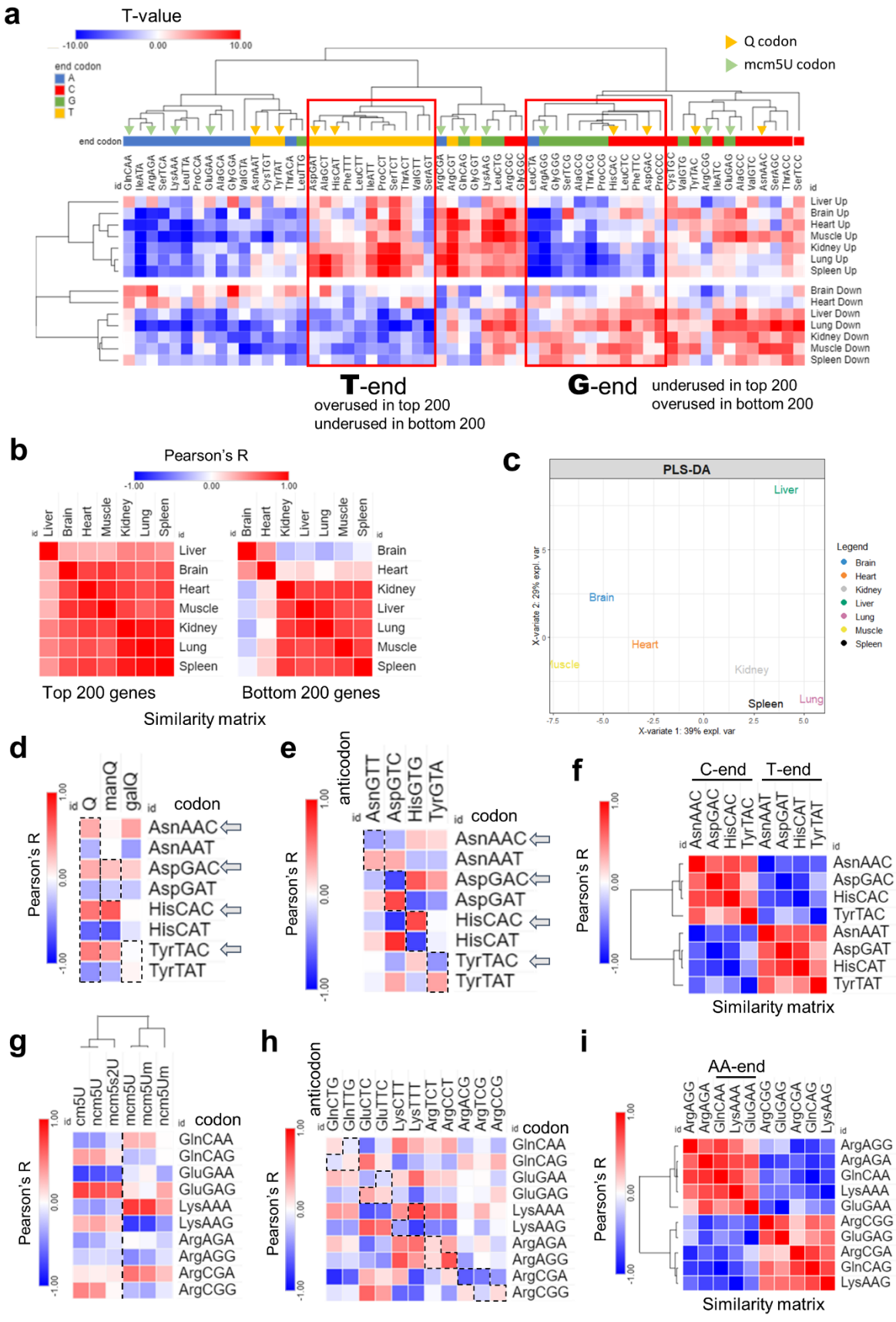

Figure 7: Analysis of total codon frequency. a: Heatmap of codon frequency in each tissue. T-stats were calculated using frequency of total codon counts in the top 200 counted genes (up) or bottom 200 genes (down). b: Heatmap of Pearson's correlation coefficients among 7 tissues by codon frequency from top (left) and bottom (right) 200 genes. c: PLS-DA analysis of tissue clustering patterns. d, e: Pearson's correlation analysis of codon frequency and Q modification enrichment (d) or Q related anticodons (e). f: Pairwise correlation analysis of Q codon from figure 7a. g, h: Pearson's correlation analysis of codon frequency and mcm5U and similar modification enrichment(g) or mcm5U related anticodons. i: Pairwise correlation analysis of mcm5U codon from figure 7a.

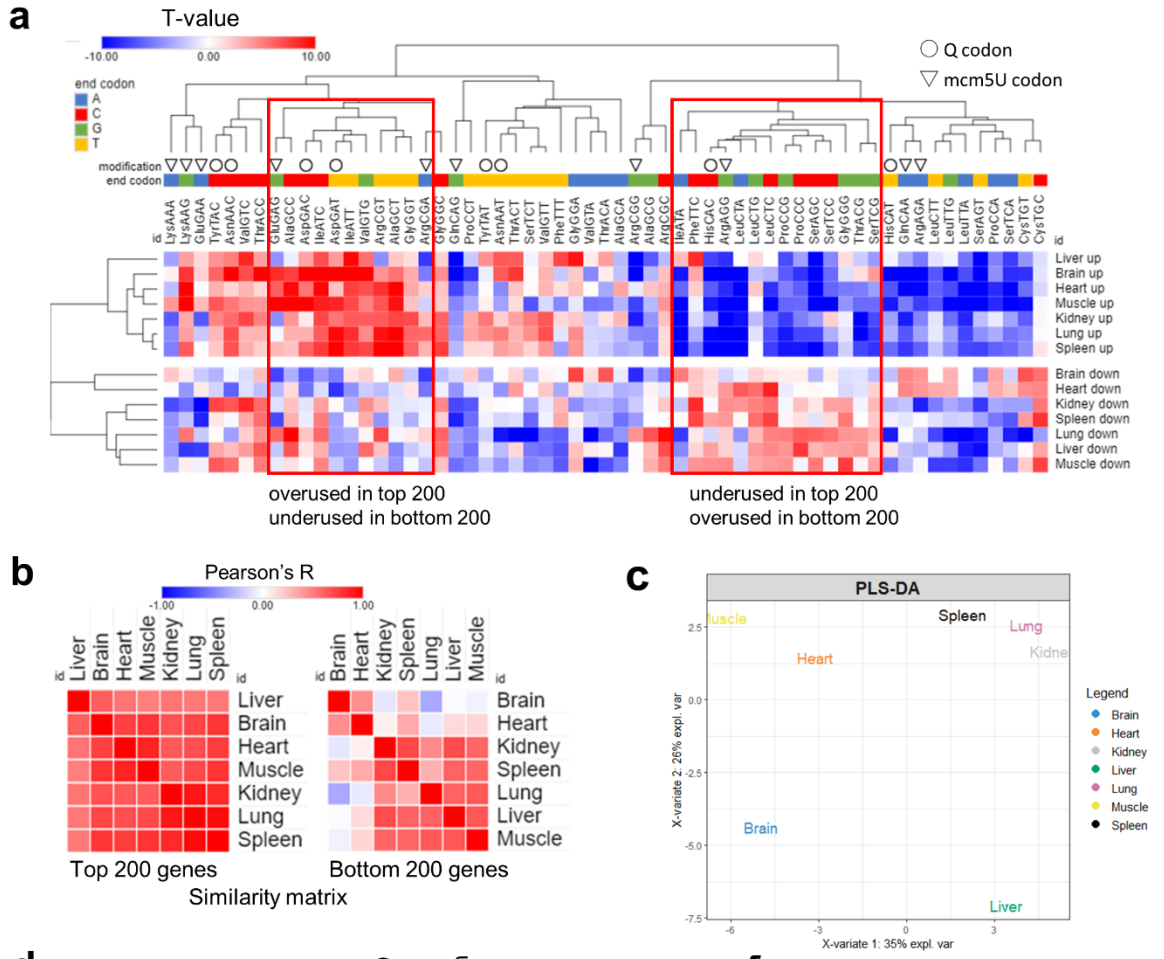

Figure 8: a: Heatmap of A-site ribosome pausing analysis. The relative dwelling time in the brain compared to other tissues is represented as log 2-fold change (log2FC). b, c: Picked up the codons related to Q modifications (c) or mcm5U modifications (d) from figure 8a. d: Pearson's correlation coefficient analysis between tissues from figure 8a.